Rhodium Supported Hβ Zeolite for the Hydrogenation of Toluene

Kalpesh B. Sidhpuria,[†,‡] Parimal A. Parikh,[§] Pratap Bahadur,[‡] and Raksh V. Jasra*[,⊥]

Discipline of Inorganic Materials and Catalysis, Central Salt & Marine Chemicals Research Institute, G. B. Marg, Bhavnagar 364 002, Gujarat, India, Department of Chemistry, Veer Narmad South Gujarat University, Surat 395 007, Gujarat, India, Chemical Engineering Department, Sardar Vallabhbhai National Institute of Technology, Surat 395 007, Gujarat, India, and R & D Centre, Reliance Industries Limited, Vadodara Manufacturing Division, Vadodara, 391 346, Gujarat, India

Noble metal Rh supported on a large pore high acidic zeolite Hβ has been explored as a hydrodearomatization catalyst. The detail kinetic study of hydrodearomatization of toluene over a 1 wt % Rh/Hβ was done in a continuous-downflow stainless steel catalytic fixed bed reactor at varied space time, toluene feed rate, hydrogen partial pressure, hydrogen to toluene mole ratio, temperature, and in the presence of dibenzothiophene. The time on stream data and reaction order with respect to toluene were measured and was found to be of first order. Fourier transform infrared (FTIR) spectra and chemical analysis of fresh and spent catalyst suggested the presence of surface carbon species and weight percent carbon was found to be 4.43%. It was observed that toluene conversion was increased on increasing H_2 partial pressure and H_2/feed mole ratio. The conversion is dependent on temperature and shows a well-defined maximum. The decrease of the catalyst activity in the presence of dibenzothiophene is mainly attributed to the adsorption and decomposition of dibenzothiophene (DBT) on the metal sites, which results in a loss of metal surface available for the reaction to take place and a higher coke formation reducing the fraction of acid sites available for toluene hydrodearomatization. A nonlinear semiempirical kinetic model was also developed to have the best fit with 12% error.

1. Introduction

In recent years, considerable attention has been paid to develop new catalysts and processes for aromatics saturation in diesel fuel. Technically, the aromatics impart poor ignition quality and low cetane number to diesel and enhances the smoke point of jet fuel and increased emission of particulate matters. These particulate matters as well as aromatics emissions are environmental hazards, and these are known to be responsible for various diseases when inhaled by humans. Therefore, stringent environmental regulations are being directed to lower these hazardous emissions from vehicle exhausts. Consequently, this along with the growing demand for high quality diesel fuels has brought hydrotreating processes center stage in the modern refinery strategies.[1] Moreover, decreasing the aromatic content results in an increase in the cetane number of the diesel. For example, typically, an aromatic reduction of 10 wt % results in a cetane number increase of 3−3.5.[2] European Union (EU) regulations for auto oil diesel standards, having come in compliance from 2005, include reduction of aromatic content to a value of 10–20 vol %.[3]

The drawbacks of the conventional hydrotreating catalysts include severe operating conditions such as high temperatures, low space velocities, high pressures, and hydrogen/feed mole ratios to achieve acceptable aromatic reduction. The hydrodearomatization reaction is reversible and at normal hydrotreating conditions, complete conversion is not possible because of equilibrium limitations. Furthermore, conventional hydrotreating catalysts comprising sulfided mixed oxides (Ni−Mo, Ni−W, Co−Mo) can only accomplish moderate levels of aromatic saturation under typical hydrotreating conditions in a single-stage operation.[4–6] Using these systems, increasing operation severity (temperature and pressure) do not result in deep levels of aromatics saturation because of thermodynamic limitations. Therefore, noble-metal based catalysts are preferred for aromatic saturation since they can work at lower temperatures, thus avoiding the thermodynamic constraints encountered with the sulfided oxides. However, noble-metal hydrogenation catalysts are sensitive and get poisoned by small amounts of sulfur and nitrogen containing hetro organic compounds normally present in the feed.[7] It is reported that high intrinsic activity and sulfur tolerance may be enhanced by deposition of noble metal on acidic supports. Recently, Song[8] proposed a design concept for unique acidic zeolites as supports for noble metals that utilizes shape-selective exclusion, hydrogen spillover, and two types of sulfur resistance. Such zeolite supports can be used to prepare bimodal distributions of noble metal particles.

Pt−Pd bimetallic supported on large pore β-zeolite have been claimed[9] to display dearomatization/cetane improvement. Lee and Rhee[10] recently reported a simultaneous decrease in the metal dispersion and hydrogenation activity of this catalyst, induced by platinum sulfide formation followed by coke deposition. The large pore zeolites preferably allow fast diffusion and reaction of bulky aromatic compounds.

It is known that noble metals deposited on acidic supports show higher turnover frequencies (TOF) compared to those supported on nonacidic supports. This has been related either to the polarization of the metal particles by nearby cations or to a metal–support interaction, which might induce a partial electron transfer between the metal and the oxide ions,[11] or between the metal and the zeolite protons.[12,13] In the latter case, the formation of the more reactive metal-proton adducts $[M_n-H_z]^{z+}$ has been proposed. [12,13] The positive effect of the acidity on the noble metal sulfur resistance was explained by the changes in the metal electron deficiency induced by metal/support interactions.[14–16] This effect leads to the formation of electron-deficient metal sites, which, in turn, lowers the strength

* To whom correspondence should be addressed. Tel.: +91-265-6693935. Fax: +91-265-6693934. E-mail: rakshvir.jasra@ril.com.
[†] Central Salt & Marine Chemicals Research Institute.
[‡] Veer Narmad South Gujarat University.
[§] Sardar Vallabhbhai National Institute of Technology.
[⊥] Reliance Industries Limited.

10.1021/ie8001793 CCC: $40.75
Published on Web 05/21/2008

of the sulfur−metal bond.[9,12,13] However, high acidity of zeolite is also known to favor excessive cracking and coke formation. In order to avoid it without suppressing the sulfur tolerance of catalysts, less acidic supports such as silica–alumina or nonacidic supports has been recently investigated. For example, Reinhoudt et al.[17] suggested the superior performance of silica–alumina supported Pt−Pd catalyst for second-stage deep hydrodesulfurization process. In contrast, Fujikawa et al.[18] reported that bimetallic Pt−Pd/silica–alumina does not improve sulfur tolerance as compared to the monometallic Pt or Pd catalysts although it significantly enhances the intrinsic activity for hydrodearomatization. Koningsberger et al.[19] investigated the potential for developing nonacidic sulfur tolerant catalyst. Rhodium supported on Hβ zeolite has not been reported so far for toluene hydrogenation in the literature.

In the present study, noble metal Rh supported on a large pore high acidic zeolite Hβ has been explored as a hydrodearomatization catalyst. Rhodium is chosen as it is relatively easy to reduce compared to other transition metals like Fe, Co and Ni.[20] Toluene was used as a model compound to simulate the aromatics in diesel fuels, because the hydrogenation of toluene is known to be more difficult than that of benzene and naphthalene. This could be related to a decrease in the resonance energy per aromatic ring as well as to differences in the π-electron cloud density in the aromatic ring as a result of the inductive effect of the methyl group.[21] Hydrogenation activity of toluene over Rh/Hβ catalyst was studied in a fixed bed reactor at varied temperatures, pressure, toluene feed rate, space-time, hydrogen-feed mole ratio, and in the presence of dibenzothiophene. A nonlinear semiempirical kinetic model is also proposed.

2. Experimental Details

2.1. Materials. A commercial Naβ zeolite (SiO_2/Al_2O_3 = 25) was obtained from Zeocat, Uetikon (Switzerland). Toluene (99.5%) and silver nitrate (99.8%) were purchased from Qualigens Fine Chemicals (India). *n*-Decane (97.0%) and ammonium chloride (99.8%) were purchased from s.d. fine Chem Ltd. (India) and Ranbaxy Fine Chemicals Limited (India), respectively. Rhodium trichloride ($RhCl_3 \cdot 3H_2O$) and dibenzothiophene (98%) were procured from Merck (Germany). Hydrogen gas (99.8%) was purchased from Alchemie Gases and Chemicals Pvt. Ltd. (India).

2.2. Preparation of Catalyst. A commercial Naβ zeolite was treated with 1 M NH_4Cl solution (zeolite to NH_4Cl solution ratio 1:80) at 353 K for 4 h. The mixture was cooled and filtered after the treatment. Solid obtained was washed with deionized water till the filtrate was free from chloride ions (checked by $AgNO_3$ test). Thus washed solid was dried in an oven at 378 K. This procedure was repeated to ensure complete exchange of Na by NH_4 ions. NH_4-exchanged zeolite was calcined in furnace for 4 h at 823 K in air to obtain the protonic form (H-form) of β zeolite. The Rh metal was supported on Hβ by impregnating 1 wt % aqueous $RhCl_3.3H_2O$ solution on the surface of Hβ. The solution containing the $RhCl_3 \cdot 3H_2O$ was added dropwise to the slurry of zeolite and stirred for 6 h. The sample was then dried in an air oven overnight at 378 K and finally calcined in air at 723 K for 4 h. The sample prepared thus was designated as Rh/Hβ.

2.3. Catalyst Characterization. The relative crystallinity of the Hβ sample was determined by X-ray diffraction (Phillips X'PERT MPD system, The Netherlands) using Cu Kα radiation (λ= 1.5405 Å) by comparing the peak area at $2\theta = 22°$ with that for the starting Naβ zeolite.

The textural properties of the catalyst were determined from N_2 adsorption–desorption isotherms at 77.4 K over the whole range of relative pressures, using ASAP-2010, Micromeritics (USA).

The particle size distribution (dry) was measured using Mastersizer 2000, Malvern (UK) at 50% feed rate and 1 bar pressure.

The electron microscopy study was carried out to examine the morphology of the catalyst with a scanning electron microscope (Leo 1430 VP, Germany) having silicon detector under a pressure of $> 1.34 \times 10^{-2}$ Pa. The samples were coated with gold using a Polaron Sputter Coater.

IR spectra of the fresh and spent catalyst samples were recorded with Perkin-Elmer Spectrum GX Fourier transform infrared (FTIR) spectrophotometer (USA) in the region of 400–4000 cm^{-1} with a resolution of 4 cm^{-1} using KBr pellet technique.

The weight percent of coke formed after the reaction was determined by the Perkin-Elmer-2400 CHNS/O (USA) analyzer.

2.4. Catalyst Activity Measurements. Hydrogenation of aromatic compound was performed in a microprocessor based continuous-downflow stainless steel catalytic fixed bed reactor (i.d. 15 mm and length 524 mm) system with PC-PLC (programmable logic controller) operating through Ellipse SCADA Software supplied by M/S, Chemito Technologies Pvt. Ltd. (India), with the ability to operate up to 5 MPa pressure and 923 K temperature, equipped with high pressure piston pump (Knauer, Germany). The schematic diagram is shown in Figure 1. The catalyst bed was diluted with glass beads to avoid dispersion effect and to obtain a homogeneous thermal distribution in the reactor. [22,23] The catalyst (0.5–2.06 mm size) was sieved and kept at the center of reactor throughout the kinetic study. The exact length of the catalytic bed was 5–6 mm when the amount of catalyst is 0.5 g. The remaining space of catalyst bed at the top and the bottom of reactor were filled with glass beads (2–4 mm) to avoid the entrance and exit effects.

Catalyst was reduced in situ by hydrogen at 723 K for 2 h. The reactor was brought to the desired temperature before the reactant was introduced. Toluene hydrogenation was carried out at different temperature (413–498 K), hydrogen pressure (1–4 MPa), toluene feed rate (0.062–0.123 mol/h), hydrogen to toluene mole ratio (3–12) and varied concentration of dibenzothiophene (50–200 ppm). Liquid sample was withdrawn from the sample-collecting vessel and analyzed by gas chromatograph (Shimadzu17A, Japan) equipped with a flame ionization detector (FID) and 5% diphenyl and 95% dimethyl siloxane universal capillary column (60 m length and 0.25 mm diameter) at appropriate times. The initial GC column temperature was increased from 313 to 473 K at the rate of 10 K/min. Nitrogen gas (3.4 mL/min) was used as a carrier gas. The temperature of injection port and FID were kept constant at 473 K during product analysis. The retention times for different compounds were determined by injecting pure compounds under identical GC conditions. *n*-Decane was used as an internal gas chromatography (GC) standard.

3. Results and Discussion

3.1. Catalyst Characterization. The relative crystallinity and textural properties data of the Naβ, Hβ, and Rh/Hβ are presented in Table 1. Partial loss of crystallinity in zeolite structure upon cation exchange in Naβ is observed (Figure 2). Similar loss in crystallinity after cation exchange in zeolite Naβ has also been reported in the literature.[24] The textural properties of the Naβ, Hβ and Rh/Hβ were evaluated from the nitrogen adsorption-

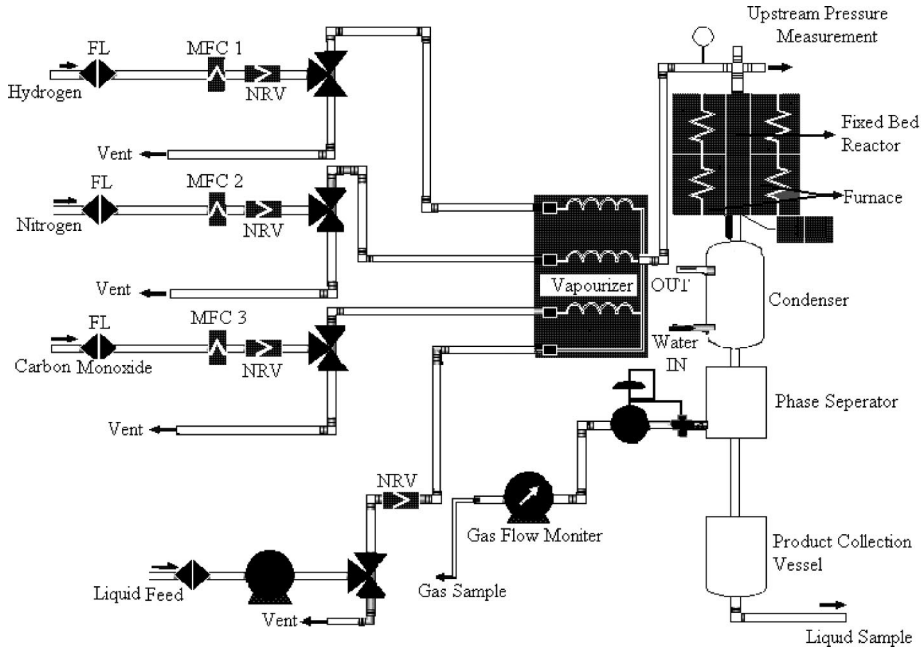

Figure 1. Schematic diagram of the catalytic fixed bed reactor.

Table 1. Relative Crystallinity and Textural Properties of Naβ, Hβ, and Rh/Hβ

sample	crystallinity (%)	BET surface area (m^2/g)	total V_p (cm^3/g)	average pore diameter (Å)	micropore volume (cm^3/g)
Naβ	100	539	0.39		0.17
Hβ	87.8	523	0.40	9.96	0.16
Rh/Hβ	84.4	562	0.44	7.40	0.17

–desorption isotherms (Figure 3A−C). Nitrogen adsorption–desorption isotherms of the Naβ, Hβ, and Rh/Hβ are of type I as per IUPAC classification,[25] whereas hysteresis belongs to type H3. The hysteresis loop of Hβ was rather flat and extended over a large range of relative pressures, which is characteristic of a microporous material. The micropore volume mentioned in Table 1 has been calculated using t-plot method. Some mesoporosity also appeared to be present in the samples. The hysteresis loops in isotherms clearly indicates that Naβ contains fewer mesopores compared to Hβ and Rh/Hβ, with the order of number of mesopores as Naβ < Hβ < Rh/Hβ. Mesoporosity observed for Hβ and Rh/Hβ is due to amorphous material formed during Na^+ exchange with proton and loss of crystallinity that is also reflected in the powder XRD data (Table 1).

The pore structure of the zeolite β consists of 12-membered rings interconnected by cages, which are formed by the intersections of the channels. The pore opening in the linear channel is ca. 0.57 nm × 0.75 nm. The tortuous channel system is formed by the intersections of the two linear channels and has a pore opening with an approximate dimension of 0.56 nm × 0.65 nm. [26] Pore size distributions were derived from numerical analysis of the N_2 adsorption data using the micropore (MP) method. The average pore diameter determined thus for the Hβ and Rh/Hβ are given in Table 1.

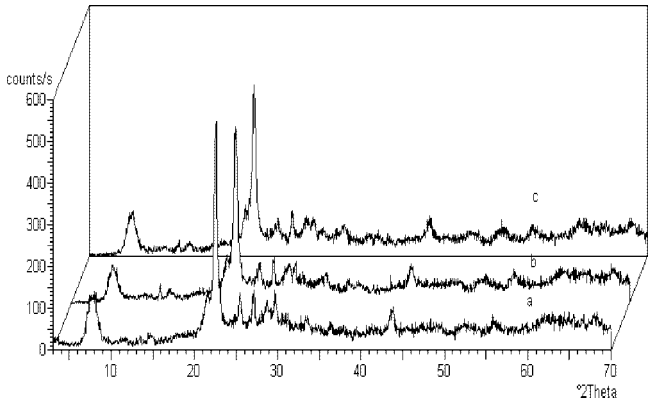

Figure 2. Powder X-ray diffraction (PXRD) patterns of (a) Naβ, (b) Hβ, and (c) Rh/Hβ.

The particle size distributions of Naβ demonstrated narrow particle size distributions within 0.5 to 9.4 μm range with an average particle size of about 1.65 μm. After cation exchange process, the particle size distribution in Hβ sample increased and observed in the range of 0.5−11.5 μm with increasing in the average particle size (~1.75 μm), while Rh metal supported Hβ zeolite showed broader particle size distributions with all particles less than ~50 μm with an average particle size of 1.87 μm. This aggregation of particles in Hβ sample may be due to the dealumination taking place during the cation exchange process,[24] while in the Rh/Hβ the aggregation of the particles occur due to the impregnation and calcination processes.

The scanning electron microscope (SEM) micrographs of Naβ sample (Figure 4A) exhibit distinct particles with less than 2 μm size, whereas Hβ (Figure 4B) and Rh/Hβ (Figure 4C) sample graphs display aggregated particles, which is in good agreement with the particle size distribution results. These aggregated particles may be due to the dealumination taking place during the cation exchange process with amorphous alumina binding the zeolite particles. It has already been reported[24,27] that dealumination in zeolite β occurs easily during the cation exchange and calcination processes.

3.2. Surface Carbon Species. The IR spectra of fresh (A) and spent (B) catalysts are shown in Figure 5. Coke formation during on-stream operation on Rh/Hβ was confirmed by the observation of bands at 1613, 1516, 1460, 1396, and 1382 cm^{-1} in spent catalyst. Similar bands were observed for zeolite materials with acidic hydroxyls.[28] However, the three bands (1460, 1396, and 1382 cm^{-1}) are attributed to CH deformation modes of $–CH_2–$ and $–CH_3$ groups. The bands at 1516 cm^{-1} is due to the deposition of product methylcyclohexane on the surface of spent catalyst.[29] The band at 1613 cm^{-1} shows the

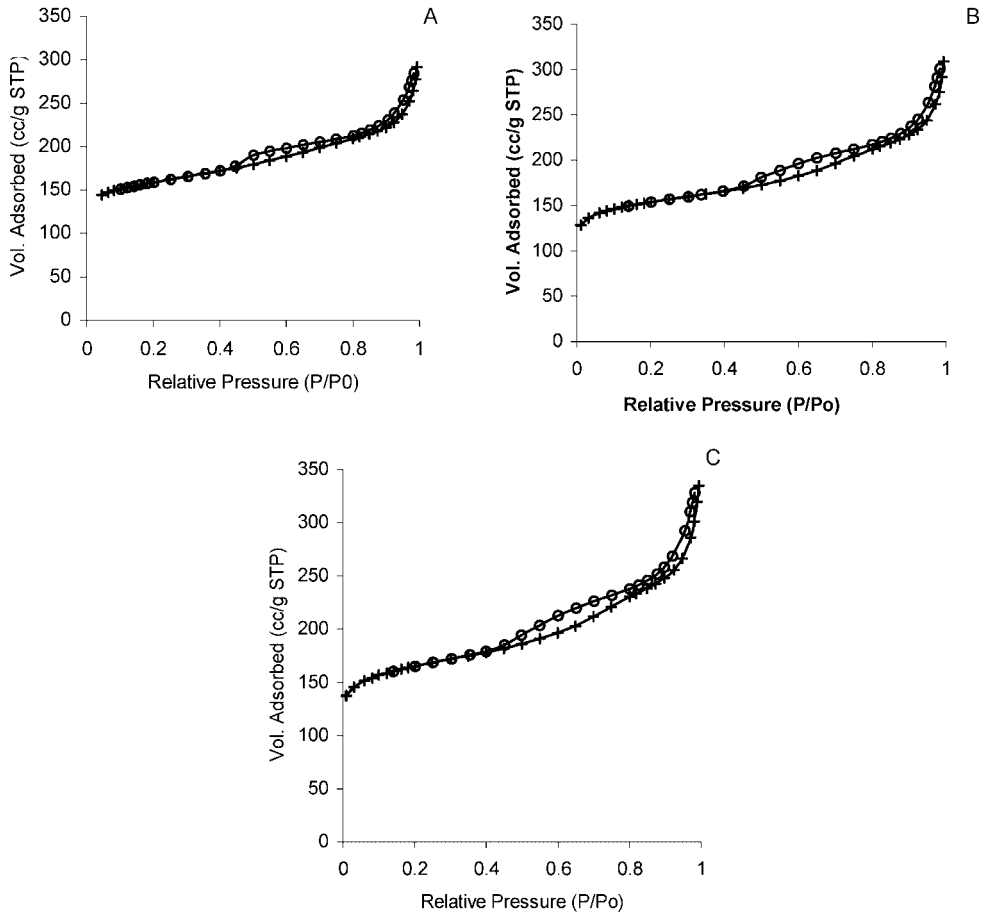

Figure 3. N_2 adsorption (+) and desorption (O) isotherms for (A) Naβ, (B) Hβ, and (C) Rh/Hβ.

presence of coke forming sites.[30] It is proposed that coke formation on beta zeolite proceeds through Lewis acid sites (Al^{3+}), while Brønsted acid sites (H^+) are required for the hydride transfer reaction.

The quantitative analysis of the deposited coke was done using CHNS/O analyzer. Spent catalyst was kept in an oven at 388 K for 4 h to desorb entrapped hydrocarbons before analyzing the coke content and composition. The carbon contents of fresh and spent catalysts were measured using acetanilide as a reference standard. The difference in carbon contents between the fresh and spent catalyst was observed to be 4.43 wt %. The acid sites of the support Hβ is responsible for the formation of unsaturated compounds (i.e., coke precursors), which undergo polymerization and cyclization to form coke. This may be due to a deficiency of sufficient hydrogenation sites (Rh) available for the hydrogenation of the coke precursors with respect to the acid sites of the zeolite support.

3.3. Catalytic Activity. Hydrogenation of toluene was observed to occur readily within studied temperature range and the selectivity for methylcyclohexane was found to be between 92 and 95%. Other products like, 1,2- and 1,3-dimethyl cyclopentane and ethylcyclopentane were also observed due to isomerization and cracking reactions that occur because of acidity of zeolite. Catalyst deactivated with time on stream (Figure 6), but the steady state operation was obtained after ca. 120 min. Steady state performance was observed up to 360 min, and then, the catalyst deactivated gradually. The catalyst deactivation is due to the formation of coke (carbon) species on the surface of support Hβ, which was confirmed by the FTIR spectra (Figure 5) of spent catalyst. The plot of ln r vs ln C suggested that the reaction is of first order ($n = 0.993$) with respect to toluene, which is in good agreement with Lepage's[31] kinetic studies of toluene hydrogenation over sulfided Ni−W/Al_2O_3. The value of rate constant, k, is found 6.04×10^{-3} min^{-1}.

Toluene conversion at the end of the 120 min of operation was taken as a steady state conversion. It is also essential for kinetic studies that the catalytic reactor operates in the differential mode. The reactor exhibited no temperature or pressure gradients across the catalyst bed and there are no diffusional limitations for the transport of reactant and product molecules, in this condition. The steady state conversion was directly proportional to space-time W/F, where W and F are the weight of catalyst and feed rate of substrate, respectively. Figure 7 shows the effect of weight of catalyst (W) on the conversion of toluene at constant feed rate of toluene (F) 0.123 mol/h, 433 K temperature, 1 MPa pressure, and 280 mL/min hydrogen flow rate. The resulting plot is seen to be linear in the region of 0–4 g h/mol. At higher W/F values, the level of toluene conversion remained virtually constant. A definite plateau, therefore, exists at higher conversions where the increased ratio of the catalyst weight to reactant flow rate has little effect on the overall catalytic activity.

Figure 8 depicts the effect of toluene feed rate on the conversion of toluene at 433 K temperature, 2 MPa pressure, and a hydrogen/toluene mole ratio of 6. Toluene conversion was found to decrease with an increase in feed rate of toluene that can be explained by two different ways. With increase in liquid feed rate, wetted fraction of the catalyst as well as the gas–liquid and liquid–solid mass transfer coefficients also increase.[32] At lower liquid feed rate, catalyst particles are partially wetted, and under these conditions, conversion in-

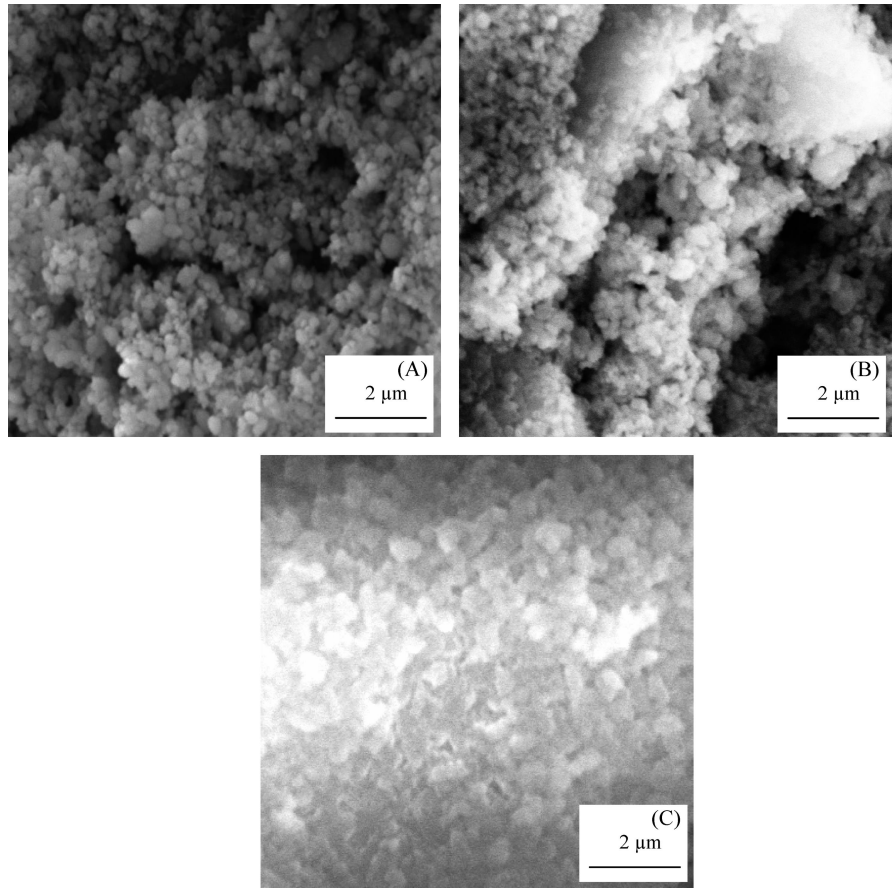

Figure 4. SEM images of (A) Naβ, (B) Hβ, and (C) Rh/Hβ.

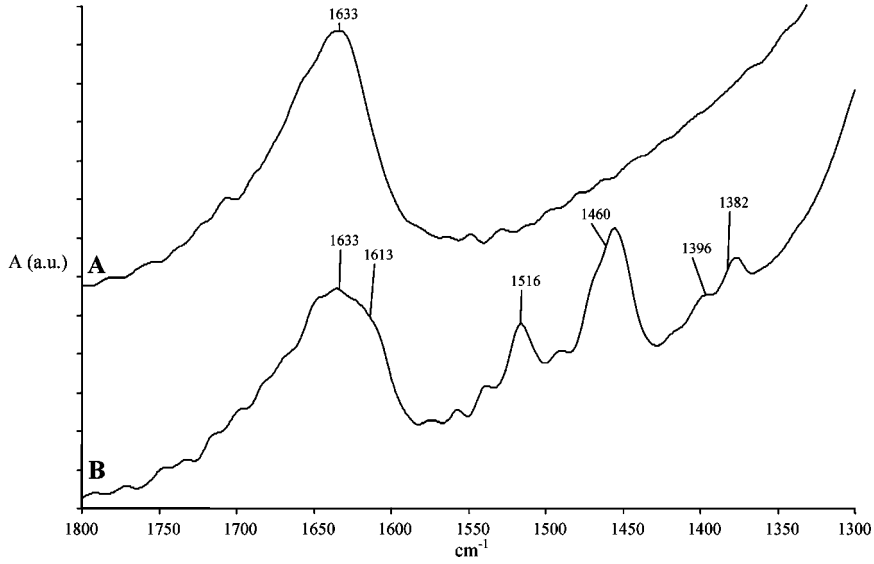

Figure 5. FTIR spectra of the fresh (A) and spent (B) Rh/Hβ catalyst.

creases due to direct transfer of the gas-phase reactant to the catalyst surface, already wetted internally due to the capillary forces. Therefore, with an increase in liquid feed rate an increase in the wetted fraction is expected to retard the conversion, while an increase in the external mass transfer coefficients will enhance the conversion. Another possible reason for observed decrease in conversion is due to the shorter residence time under high liquid flow rate. However, the former explanation is applicable to the large catalyst bed but here we are using very low amount of catalyst around 0.5 g (smaller catalyst bed), hence the latter explanation is more appropriate for this study.

It is seen that high pressures favor low equilibrium concentrations of aromatics, i.e., high conversions. This is particularly true for reactions where the number of moles of hydrogen, required for complete saturation is high. Figure 9 depicts the effect of hydrogen partial pressure on toluene conversion. The effect of hydrogen partial pressure on initial conversion was studied in the range of hydrogen partial pressure of 1–4 MPa,

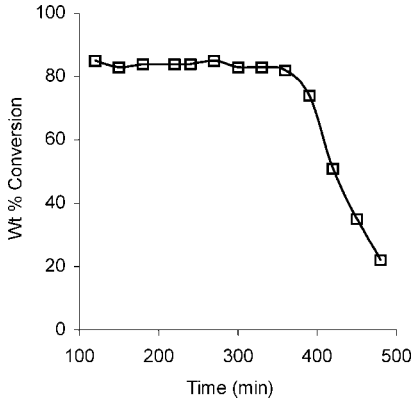

Figure 6. Time on stream measurements at $T = 433$ K, $P = 2$ MPa, toluene feed rate = 0.062 mol/h, H_2/toluene mole ratio = 6.

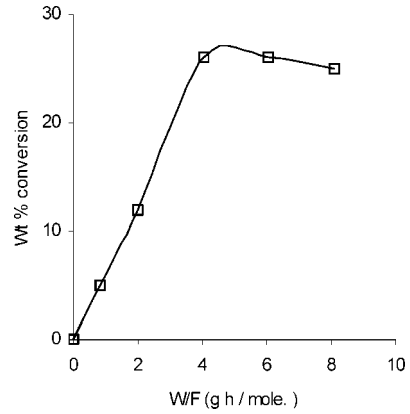

Figure 7. Effect of varying *W/F* (by changing the weight of catalyst) at temperature 433 K, feed rate of toluene 0.123 mol/h, pressure 1 MPa, and hydrogen flow rate at 280 mL/min.

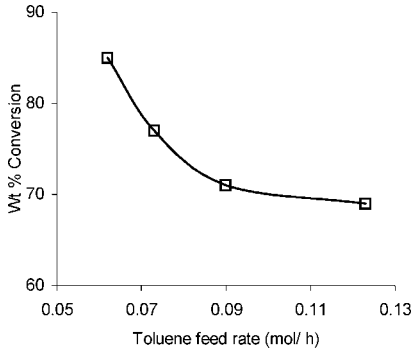

Figure 8. Effect of toluene feed rate at $T = 433$ K, $P = 2$ MPa, H_2/toluene mole ratio = 6.

at 433 K, and a toluene feed rate of 0.123 mol/h. Toluene conversion linearly increased and then remained almost constant, which indicates that hydrogen partial pressure has significant effect on hydrogenation activity. Hydrogen and aromatic hydrocarbons adsorbs on different types of sites and that the reaction occurs simultaneously on Rh surface and on acid sites in the interface region as mentioned in Scheme 1.The increase in hydrogen partial pressure increased hydrogen dissociation on the metal surface and, thus, increased the concentration of hydrogen available for toluene hydrogenation.

The effect of the hydrogen to toluene mole ratio in the range of 3–15 was studied at 433 K (Figure 10). Toluene conversion increased up to a hydrogen/toluene mole ratio of 12 and then remained constant. Toluene conversion is increased due to increase in the concentration of hydrogen on the support surface

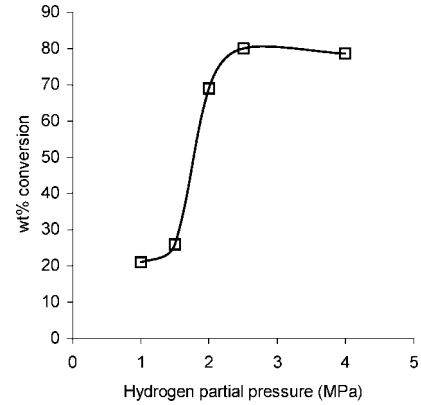

Figure 9. Effect of hydrogen partial pressure at $T = 433$ K, feed rate = 0.123 mol/h, H_2 flow rate = 280 mL/min, H_2/toluene mole ratio = 6.

Scheme 1. Some Important Steps in the Toluene Hydrogenation Reaction

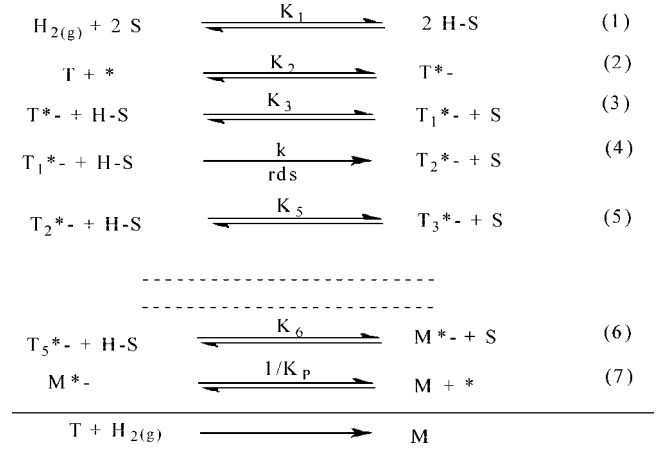

in the vicinity of the metal particles. Hence, the metal–support interface region could contribute to the overall activity of the toluene hydrodearomatization if the concentration of adsorption sites for toluene is high enough and the hydrogen transport rate is sufficiently rapid.

3.4. Kinetic Modeling. The heterogeneously catalyzed hydrodearomatization of toluene is a three phase (gas–liquid–solid catalyzed) reaction system, in which a number of steps occur in series. The solute gas hydrogen diffuses through the gas phase to the gas–liquid interface and then from the interface to the bulk liquid. Dissolved hydrogen and toluene present in the liquid phase are then transferred to the external surface of the catalyst

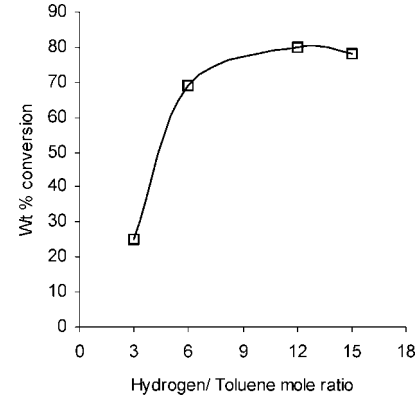

Figure 10. Effect of hydrogen to toluene mole ratio at $T = 433$ K, $P = 2$ MPa, toluene feed rate of 0.123 mol/h.

particles through the solid–liquid film. These reactants then reach on to the active centers where the reaction occurs and the product diffuses out. Doraiswamy and Sharma[33] have provided an insight into gas–liquid reactions occurring in the presence of a solid catalyst. To develop a suitable rate equation representing the intrinsic kinetic, the data were analyzed for the significance of mass transfer resistance. It was assumed that since the pure hydrogen was used, the gas mass transfer resistance is negligible.

The model proposed cannot be considered as a Langmuir–Hinshelwood (LH) mechanism because a single rate-determining step (RDS) is not proposed; however, it has many similarities to an LH model because adsorption quasi-equilibrium of reactants is assumed. [34] The proposed mechanism is presented in Scheme 1. We assume that toluene adsorbs on both Rh and zeolite support surface. The adsorbed toluene species are the most abundant surface intermediates, i.e., surface coverage of all other reaction intermediate is negligible. Hydrogen molecules adsorb on the metal site and get converted to activated hydrogen, which can migrate to the interfacial region via spillover. The reaction occurs simultaneously on both metal crystallites and acid sites in the interface region. The reactive hydrogen species are weakly bound; thus the coverage is relatively low. Desorption of methylcyclohexane is fast and irreversible from both regions.

Since approximately 75% of all heterogeneous reaction mechanisms are surface-reaction-limited rather than adsorption- or desorption-limited, we begin by assuming; the rate-determining step (RDS) is the addition of the second H atom (or the simultaneous addition of the first two atoms, possibly by an activated hydrogen molecule). In Scheme 1, S is an adsorption site for hydrogen, T is the toluene molecule, * is an adsorption site for T, Ti is an intermediate obtained after adding i number of hydrogen atoms, and M is the methylcyclohexane. The rate expression (eq 8) was derived from the actual reaction mechanism (Scheme 1), assuming eq 4 as the rate-determining step.

$$r = \frac{kK_1K_2K_3pC_T}{(1+(K_1p)^{0.5})(1+K_2C_T)} \tag{8}$$

where p is the partial pressure of hydrogen and C_T is the concentration of toluene. The terms k, K_1, K_2, and K_3 are the constants. The rate parameters from the complex rate model (eq 8) were determined by Polymath software (version 5.1). On the basis of the minimized sum of squares of the errors (ϕ_{min}) between calculated and experimental rates, we choose the best-fit model. ϕ_{min} was calculated as

$$\phi_{min} = \sum_{i=1}^{N} (\text{rate}_{\text{calc}(i)} - \text{rate}_{\text{exp}(i)})^2 \tag{9}$$

It was found that the experimental data do not fit properly in eq 8 since the minimized sum of root mean-squares error (ϕ_{min}) was up to 35%. Therefore, this model was discarded for present system.

Complicated rate equations with a large number of parameters can also be derived by assuming various steps as rate controlling step with different adopted simplifications. In this case, more unknown parameters should be evaluated from experimental data, and reliable parameters values would be obtained. Therefore, it is preferred to introduce simplified semiempirical rate equation, which is consistent with the observed reaction behavior, and rate eq 10 was found to be the best representing our experimental data. Values of k_{Rh} ($k_{Rh} = kK_3$), K_1, and K_2 of eq 10 are found to be 9997.74 1/h, 67.80×10^{-3} 1/MPa, and 17.95×10^{-3} mol/L, respectively at 433 K.

$$r = \frac{k_{Rh}(K_1p)^{3.1}K_2C_T}{(1+(K_1p)^{3.1}(1+K_2C_T)} \tag{10}$$

which have minimized sum of root-mean-squares deviation (variance), 4.256×10^{-7}, and an average error between experimental and calculated rates was found to be 12%, which is in the kinetic range.

3.5. Effect of Temperature. A maximum in toluene conversion as a function of temperature was observed. The activity for toluene hydrogenation passes through a maximum near 433 K (Figure 11). Similar kind of behavior has been reported for toluene hydrogenation by others.[35–37] The maxima for toluene hydrogenation is reversible and can be traversed from either the high or low temperature side, which implies that it is not due to catalyst deactivation. Also, this is not a consequence of thermodynamic limitations because the conversions were far from equilibrium conversions. The occurrence of this maximum for toluene hydrogenation has been explained by the continued decrease in the aromatic hydrocarbon surface coverage as temperature increases, which at some point becomes small enough to noticeably decrease the conversion.[35] Also, at high temperature, poisoning of the catalyst surface by organic residue is possible.[38]

3.6. Sulfur Poisoning of Catalyst. A solution of toluene and different level of dibenzothiophene (DBT) concentration (50, 100, and 200 ppm), as a sulfur source, was used to measure the sulfur tolerance of the catalyst at 433 K temperature, 2 MPa pressure, and 0.062 mol/h feed rate of solution (Figure 12). Toluene conversion was observed to decrease with increasing the DBT concentration. Without DBT, steady state performance was observed up to 360 min and then catalyst deactivated gradually, while increasing the concentration of DBT from 0 ppm to 50, 100, and 200 ppm the catalyst was deactivated after 240, 210, and 180 min, respectively. The decrease of the catalyst activity in the presence of DBT is mainly attributed to the adsorption and decomposition of DBT on the metal sites, which results in a loss of metal surface available for the reaction to take place and a higher coke formation reducing the fraction of acid sites available for toluene hydrodearomatization. It is reported that the thiophene decomposition increases with increasing the acid site concentration, thus increasing the formation of H_2S and the coke precursor species on the catalyst.[39] Hence, the rapid deactivation of Rh/Hβ catalyst was caused by three different mechanisms, i.e., a metal sulfur poisoning by dibenzothiophene adsorption, a metal sulfur poisoning by H_2S adsorption and an enhanced coke formation induced by the presence of the unsaturated hydrocarbon species,

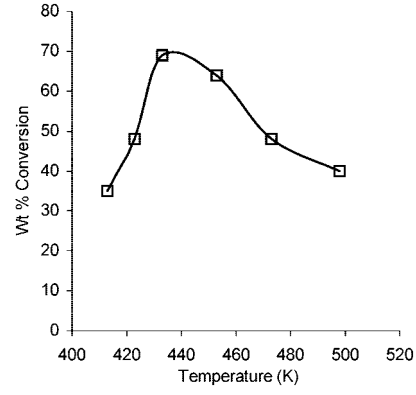

Figure 11. Effect of temperature at pressure 2 MPa, toluene feed rate 0.123 mol/h, H_2 flow rate = 280 mL/min, and H_2/feed mole ratio = 6.

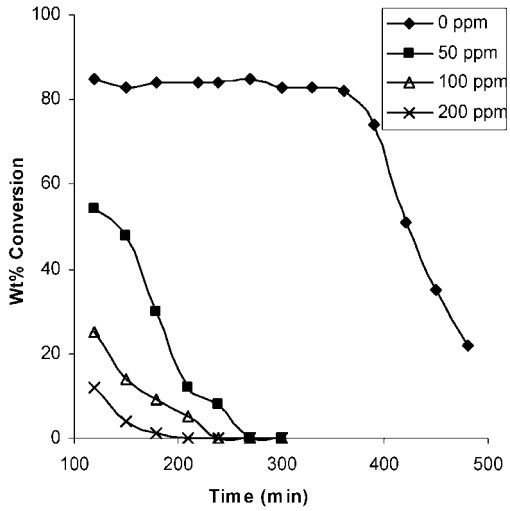

Figure 12. Effect of dibenzothiophene (DBT) on catalytic activity of Rh/Hβ with time on stream at T= 433 K, P = 2 MPa, toluene feed rate = 0.062 mol/h, H_2/toluene mole ratio = 6.

which were produced by decomposition of dibenzothiophene on the acid sites.

4. Conclusions

Hβ material having high surface area and a regular arrangement of uniform pores is a good support for preparing Rh supported catalyst. The kinetics and catalytic behavior of the hydrodearomatization of toluene over 1 wt % Rh/Hβ are reported. The reaction order with respect to toluene was found to be first order. The Rh/Hβ shows good activity in the hydrogenation of toluene. This is not only due to the higher metal content, but also due to the acid sites of the zeolite, which participate in the hydrogen spillover mechanism. However, coke formation simultaneously occurs on the acid sites of the zeolite and weight percent coke was found to be 4.43%.

The conversion is dependent on temperature and shows a well-defined maximum. The temperature maximum is explained by adsorption phenomena and the observed shift in the maximum by a self-poisoning step. The decrease of the catalyst activity in the presence of dibenzothiophene is mainly attributed to the adsorption and decomposition of DBT on the metal sites, which results in a loss of metal surface available for the reaction to take place and a higher coke formation reducing the fraction of acid sites available for toluene hydrodearomatization. The nonlinear semiempirical kinetic model representing the data was found to be the best with 12% error between experimental and calculated rates.

Acknowledgment

Authors are thankful to the Director, CSMCRI, for providing necessary facilities and also Mr. S.K. Sharma for useful discussions.

Literature Cited

(1) Corma, A.; Martinez, A.; Martinez-Soria, V. Hydrogenation of Aromatics in Diesel Fuels on Pt/MCM-41 Catalysts. *J. Catal.* **1997**, *169*, 480.

(2) Pulikottil, A. C.; Manna, U.; Santra, M.; Verma, R. P. Role of Catalyst to Meet Challenges of New Fuel and Lube Base Stock Specifications in Petroleum Refining Industry. *Bull. Catal. Soc. India* **2002**, *1*, 9.

(3) Courty, P.; Gruson, J. F. Refining Clean Fuels for the Future. *Oil Gas Sci. Technol.−Rev. IFP* **2001**, *56*, 515.

(4) Stanislaus, A.; Cooper, B. H. Aromatic Hydrogenation Catalysis: A Review. *Catal. Rev. Sci. Eng.* **1994**, *36*, 75.

(5) Cooper, B. H.; Donnis, B. B. L. Aromatic Saturation of Distillates: An Overview. *Appl. Catal. A: Gen.* **1996**, *137*, 203.

(6) Cooper, B. H.; Stanislaus, A.; Hannerup, P. N. Diesel Aromatic Saturation: A comparative Study of Four Catalyst Systems. *ACS National Meeting*, San Francisco, April 1992.

(7) Barbier, J.; Lamy-Pitara, E.; Marecot, P.; Boitiaux, J. P.; Cosyns, J.; Verna, F. Role of Sulfur in Catalytic Hydrogenation Reactions. *Adv. Catal.* **1990**, *37*, 279.

(8) Song, C.; Ma, X. New Design Approaches to Ultra-clean Diesel Fuels by Deep Desulfurization and Deep Dearomatization. *Appl. Catal. B: Environ.* **2003**, *41*, 207.

(9) Kukes, S. G.; Clark, F. T.; Hopkins, D. *Distillate Hydrogenation*. WIPO Patent, WO 94/19429, 1994.

(10) Lee, J. K.; Rhee, H. K. Sulfur Tolerance of Zeolite Beta- Supported Pd-Pt Catalysts for the Isomerization of n-Hexane. *J. Catal.* **1998**, *177*, 208.

(11) De Mallmann, A.; Barthomeuf, D. Correlation Between Benzene Hydrogenation Activity and Zeolite Basicity in Platinum Faujasites. *J. Chim. Phys. Phys.−Chim. Biol.* **1990**, *87*, 535.

(12) Homeyer, S. T.; Schatler, W. M. H. Elementary Steps in the Formation of Highly Dispersed Palladium in NaY: I. Pd Ion Coordination and Migration. *J. Catal.* **1989**, *117*, 91.

(13) Schatler, W. M. H.; Stakheev, A.Yu. Electron-deficient Palladium Clusters and Bifunctional Sites in Zeolites. *Catal. Today* **1992**, *12*, 283.

(14) Landau, M. V.; Kruglikov, V.Ya.; Goncharova, N. V.; Konoval'chikov, O. D.; Chukin, G. D.; Smirnov, B. V.; Malevich, V. I. Study of the Nature of the Interaction of the Metal Component with the Support in Metal-Zeolite Catalysts: II. Sulfur Resistance of the Metal Component in Palladium Zeolite Catalysts of Hydrogenation. *Kinet. Catal.* **1976**, *17*, 1281.

(15) Marecot, P.; Mahoungou, J. R.; Barbier, J. Benzene Hydrogenation on Platinum and Iridium Catalysts. Variation of the Toxicity of Sulfur with the Nature of the Support. *Appl. Catal. A: Gen.* **1993**, *101*, 143.

(16) Miller, J. T.; Koningsberger, D. C. The Origin of Sulfur Tolerance in Supported Platinum Catalysts: The Relationship between Structural and Catalytic Properties in Acidic and Alkaline Pt/LTL. *J. Catal.* **1996**, *162*, 209.

(17) Reinhoudt, H. R.; Troost, R.; van Langenveld, A. D.; van Veen, J. A. R.; Sie, S. T.; Moulijn, J. A. Testing and Characterization of Pt/ASA and PtPd/ASA for Deep HDS reactions. *Stud. Surf. Sci. Catal.* **1999**, *127*, 251.

(18) Fujikawa, T.; Idei, K.; Ebihara, T.; Mizuguchi, H.; Usui, K. Aromatic Hydrogenation of Distillates over SiO_2-Al_2O_3-Supported Noble metal Catalysts. *Appl. Catal. A: Gen.* **2000**, *192*, 253.

(19) Miller, J. T.; Mojet, B. L.; Ramaker, D. E.; Koningsberger, D. C. A New model for the Metal-Support Interaction: Evidence for a Shift in the Energy of the Valence Orbitals. *Catal. Today* **2000**, *62*, 101.

(20) Vishwanathan, V.; Rajashekhar, M. S.; Sreekanth, G.; Narayanan, S. Comparative Investigation of Hydrogen Chemisorption and Benzene Hydrogenation Activity of Supported Rhodium Catalysts. *J. Chem. Soc., Faraday Trans.* **1991**, *87*, 3449.

(21) Moreau, C.; Geneste, P. In *Theoretical Aspects of Heterogeneous Catalysis*; Moffat, J. B., Ed.; Van Nostrand Reinhold: New York, 1990; p 256.

(22) Tsai, M. C.; Chen, Y. W.; Kang, B. C.; Wu, J. C.; Leu, L. J. Hydrodesulfurization and Hydrodemetalation Reactions of Residue oils over CoMo/Aluminum Borate Catalysts in a Trickle Bed Reactor. *Ind. Eng. Chem. Res.* **1991**, *30*, 1801.

(23) Klinken, J. V.; Dongen, R. H. V. Catalyst Dilution for Improved Performance of Laboratory Trickle-flow Reactors. *Chem. Eng. Sci.* **1980**, *35*, 59.

(24) Sheemol, V. N.; Tyagi, B.; Jasra, R. V. Acylation of Toluene using Rare Earth Cation Exchanged Zeolite β as Solid Acid Catalyst. *J. Mol. Catal. A: Chem.* **2004**, *215*, 201.

(25) Gregg, S. J., Sing, K. S. W., Eds. *Adsorption, Surface Area and Porosity*, 2nd ed.; Academic Press: London, 1982.

(26) Tracy, M. M.; Newsan, J. M. Two new Three-dimensional Twelve-ring Zeolite Frameworks of which Zeolite Beta is a disordered intergrowth. *Nature* **1988**, *332*, 249.

(27) Muller, M.; Harvey, G.; Prins, R. Comparison of the Dealumination of Zeolites Beta, Mordenite, ZSM-5 and Ferrierite by Thermal Treatment, Leaching with Oxalic Acid and Treatment with $SiCl_4$ by ^1H, ^{29}Si and ^{27}Al MAS NMR. *Microporous Mesoporous Mater.* **2000**, *34*, 135.

(28) Datka, J.; Sarbak, Z.; Eischens, R. P. Infrared Study of Coke on Aluminium and Zeolites Beta. *J. Catal.* **1994**, *145*, 544.

(29) Caeiro, G.; Magnoux, P.; Ayrault, P.; Lopes, J. M.; RamoaRibeiro, F. Deactivation Effect of Coke and Basic Nitrogen Compounds During the Methylcyclohexane Transformation over H-MFI Zeolite. *Chem. Eng. J.* **2006**, *120*, 43.

(30) Pawlec, B.; Mariscal, R.; Navarro, R. M.; Bokhorst, S. van.; Rojas, S.; Fierro, J. L. G. Hydrogenation of Aromatics over Supported Pt-Pd Catalysts. *Appl. Catal. A: Gen.* **2002**, *225*, 223.

(31) Lepage, L. F. *Applied Heterogeneous Catalysis*; Technip: Paris, 1987.

(32) Chaudhari, R. V.; Jaganathan, R.; Mathew, S. P.; Julcour, C.; Delmas, H. Hydrogenation of 1,5,9- Cyclododecatriene in Fixed-Bed Reactors: Down- vs. Upflow Modes. *AIChE J.* **2002**, *48*, 110.

(33) Doraiswamy, L. K.; Sharma, M. M. *Heterogeneous Reactions: Analysis, Examples and Reactor Design*; Wiley: New York, 1984; Vol. 2.

(34) Rahaman, M. V.; Vannice, M. A. The Hydrogenation of Toluene and o-, m-, and p-Xylene over Palladium: II. Reaction Model. *J. Catal.* **1991**, *127*, 267.

(35) Rahaman, M. V.; Vannice, M. A. The Hydrogenation of Toluene and o-, m-, and p-Xylene over Palladium: I. Kinetic Behavior and o-Xylene Isomerization. *J. Catal.* **1991**, *127*, 251.

(36) Orozco, J. M.; Webb, G. The Adsorption and Hydrogenation of Benzene and Toluene on Alumina-and Silica-Supported Palladium and Platinum Catalysts. *Appl. Catal.* **1983**, *6*, 67.

(37) Bandiera, J.; Meriaudeau, P. Hydrogenation of Toluene over Pt and Pt-Cu Alloys in NaY. *React. Kinet. Catal. Lett.* **1988**, *37*, 373.

(38) Coughlan, B.; Kean, M. A. The Hydrogenation of Benzene over Nickel-Supported Y Zeolites: Part 1. A Kinetic Approach. *Zeolite* **1991**, *11*, 12.

(39) Simon, L. J.; van Ommen, J. G.; Jentys, A.; Lercher, J. A. Sulfur Tolerant Pt-Supported Zeolite Catalysts for Benzene Hydrogenation, I. Influence of the Support. *J. Catal.* **2001**, *201*, 60.

Received for review January 31, 2008
Revised manuscript received March 3, 2008
Accepted March 12, 2008

IE8001793